Aeolian Research 22 (2016) 141–151

Contents lists available at ScienceDirect

Aeolian Research

journal homepage: www.elsevier.com/locate/aeolia

Dynamics of skimming flow in the wake of a vegetation patch

Jerome R. Mayaud *, Giles F.S. Wiggs, Richard M. Bailey

School of Geography and the Environment, Oxford University Centre for the Environment, University of Oxford, Oxford OX1 3QY, UK

ARTICLE INFO

Article history:
Received 29 February 2016
Revised 25 July 2016
Accepted 1 August 2016
Available online 22 August 2016

Keywords:
Dryland vegetation
Turbulence
Wind erosion
Quadrant analysis
Aerodynamic roughness
Boundary layer

ABSTRACT

Dryland vegetation is often spatially patchy, and so affects wind flow in complex ways. Theoretical models and wind tunnel testing have shown that skimming flow develops above vegetation patches at high plant densities, resulting in little or no wind erosion in these zones. Understanding the dynamics of skimming flow is therefore important for predicting sediment transport and bedform development in dryland areas. However, no field-based data are available describing turbulent airflow dynamics in the wake of vegetation patches. In this study, turbulent wind flow was examined using high-frequency (10 Hz) sonic anemometry at four measurement heights (0.30 m, 0.55 m, 1.10 m and 1.65 m) along a transect in the lee of an extensive patch of shrubs (z = 1.10 m height) in Namibia. Spatial variations in mean wind velocity, horizontal Reynolds stresses and coherent turbulent structures were analysed. We found that wind velocity in the wake of the patch effectively recovered over ~12 patch heights (h) downwind, which is 2–5 h longer than previously reported recovery lengths for individual vegetation elements and two-dimensional wind fences. This longer recovery can be attributed to a lack of flow moving around the obstacle in the patch case. The step-change in roughness between the patch canopy and the bare surface in its wake resulted in an initial peak in resultant horizontal shear stress (τ_r) followed by significant decrease downwind. In contrast to τ_r, horizontal normal Reynolds stress ($\overline{u'^2}$) progressively increased along the patch wake. A separation of the upper shear layer at the leeside edge of the patch was observed, and a convergence of τ_r curves implies the formation of a constant stress layer by ~20 h downwind. The use of τ_r at multiple heights is found to be a useful tool for identifying flow equilibration in complex aerodynamic regimes. Quadrant analysis revealed elevated frequencies of Q2 (ejection) and Q4 (sweep) events in the immediate lee of the patch, which contributed to the observed high levels of shear stress. The increasing downwind contribution of Q1 (outward interaction) events, which coincides with greater $\overline{u'^2}$ and wind velocity, suggests that sediment transport potential increases with greater distance from the patch edge. Determining realistic, field-derived constraints on turbulent airflow dynamics in the wakes of vegetation patches is crucial for accurately parameterising sediment transport potential in larger-scale dryland landscape models. This will help to improve our understanding of how semi-vegetated desert surfaces might react to future environmental and anthropogenic stresses.

1. Introduction

The extreme nature of drylands means that semi-arid vegetation is often patchy and dynamic through time and space, due to complex relationships between plants, soil and transport processes (Meron et al., 2004; Wainwright, 2009; Bailey, 2011; Getzin et al., 2014). Vegetation elements provide drag on the overlying airflow, thus affecting wind velocity profiles and significantly complicating aeolian dynamics on desert surfaces (Ash and Wasson, 1983; Wolfe and Nickling, 1993; Wiggs et al., 1994, 1995; King et al., 2005). Shifts in vegetation structure resulting from grazing, fire and climatic changes are known to have a significant impact on the potential for sediment mobility (Li et al., 2008; Sankey et al., 2012), and therefore have important implications for landscape-scale change in many dryland systems (Thomas et al., 2005; Wang et al., 2009; Stewart et al., 2014).

Patchy dryland vegetation modulates the erodibility of the surface and the erosivity of the wind through three primary mechanisms (Wolfe and Nickling, 1993). First, vegetation can directly shelter sediment from the wind by covering a fraction of the surface and providing a lee-side wake (e.g. Al-Awadhi and Willetts, 1999; Leenders et al., 2007). Second, vegetation acts to trap windborne particles, thus reducing flux and providing loci for sediment deposition (e.g. Gillies et al., 2000, 2014; Okin et al., 2006; Davidson-Arnott et al., 2012). Finally, vegetation directly affects

* Corresponding author.
E-mail address: jerome.mayaud@gmail.com (J.R. Mayaud).

http://dx.doi.org/10.1016/j.aeolia.2016.08.001
1875-9637/

wind velocity profiles by acting as a form of roughness that results in the growth of a boundary layer downwind (Greeley and Iversen, 1985).

The impact of boundary layer growth on meso-scale erosion patterns depends strongly on the type of flow regime (Wolfe and Nickling, 1993). When isolated roughness elements populate the surface (<16% cover; Wolfe and Nickling, 1993), each plant sheds turbulent eddies by diverting windflow around and above each plant (Judd et al., 1996; Sutton and McKenna-Neuman, 2008; Suter-Burri et al., 2013; Lee et al., 2014). This increases drag, thus raising shear stress and the aerodynamic roughness (z_0), and potentially enhancing erosion locally (Ash and Wasson, 1983). An arch vortex with a reverse surface flow direction can develop directly downwind of individual elements, upwind of a flow stagnation region where the outer flow reattaches to the ground (Sutton and McKenna-Neuman, 2008; Walter et al., 2012). In wake-interference flow (c. 16–40% cover; Wolfe and Nickling, 1993), the increased drag and thus shear stress resulting from the presence of multiple elements may only be partly absorbed by the plants themselves, resulting in stress transference to the inter-canopy surface and potentially greater sediment transport (Breshears et al., 2009; Dupont et al., 2014). In the case of skimming flow (>∼40% cover; Wolfe and Nickling, 1993), the increased drag from the vegetation acts to displace z_0 upwards (establishing a zero-plane displacement height, d), which simultaneously extracts momentum from the surface wind and increases wind shear stress above the canopy (e.g. Wasson and Nanninga, 1986; Gillette and Stockton, 1989; Wiggs et al., 1994; Gillies et al., 2002; Crawley and Nickling, 2003; Gillette et al., 2006; Dupont et al., 2014). The absorption of additional stresses by the plants therefore decreases the erosion potential at the surface. Fig. 1 displays the different flow regimes and their associated theoretical wake developments.

Theoretical calculations (e.g. Raupach, 1992; Okin, 2008) and experimental measurements (Minvielle et al., 2003; Leenders et al., 2007; Youssef et al., 2012; Gillies et al., 2014; Wu et al., 2015; Mayaud et al., 2016) suggest that protective wakes downwind of individual vegetation elements extend to approximately 7–10 h (where h is the height of the element). Wind dynamics in the wakes of more substantial vegetation patches, where skimming flow is in operation, are less well studied, excepting some wind tunnel studies (e.g. Burri et al., 2011; Youssef et al., 2012; Suter-Burri et al., 2013) and a few field and modelling studies of forest edges (e.g. Gash, 1986; Liu et al., 1996; Frank and Ruck, 2008). Belcher et al. (2003) provided a useful model for describing the adjustment of a turbulent boundary layer to the step-change in surface roughness represented by a forest patch, focusing mainly on the above-canopy zone. Wind tunnel and modelling experiments have also been conducted to understand flow behaviour around backward-facing steps (e.g. Le et al., 1997; Wengle et al., 2001), although these configurations often have more extensive low-velocity zones and delayed reattachment points compared to vegetated cases due to their almost parallel-to-wall streamlines. To our knowledge no field-based study has characterised flow recovery and turbulence in the wake of a real dryland vegetation patch. This is a significant gap in the literature, given the increasing evidence that high-frequency turbulence is an important driving force behind aeolian sediment entrainment and transport in the boundary layer (Butterfield, 1991; Sterk et al., 1998; Namikas et al., 2003; Schönfeldt and von Löwis, 2003; Baas and Sherman, 2005; Leenders et al., 2005; Baddock et al., 2011; Weaver and Wiggs, 2011; Wiggs and Weaver, 2012; Chapman et al., 2013).

Wind erosion models form a key part of our understanding of sediment transport dynamics on partly vegetated surfaces, and are crucial for assessing the potential vulnerability of dryland regions to soil degradation (Okin et al., 2006; Ravi et al., 2011). A wind erosion model presented by Okin (2008) recognises the inherent irregularity of vegetation patterning in drylands, and emphasises the controlling influence of the size of 'gaps' or 'corridors' in the vegetation structure. The Okin model assumes that plants are porous objects, such that surface shear velocities in the wake of plants can be greater than zero and recover asymptotically.

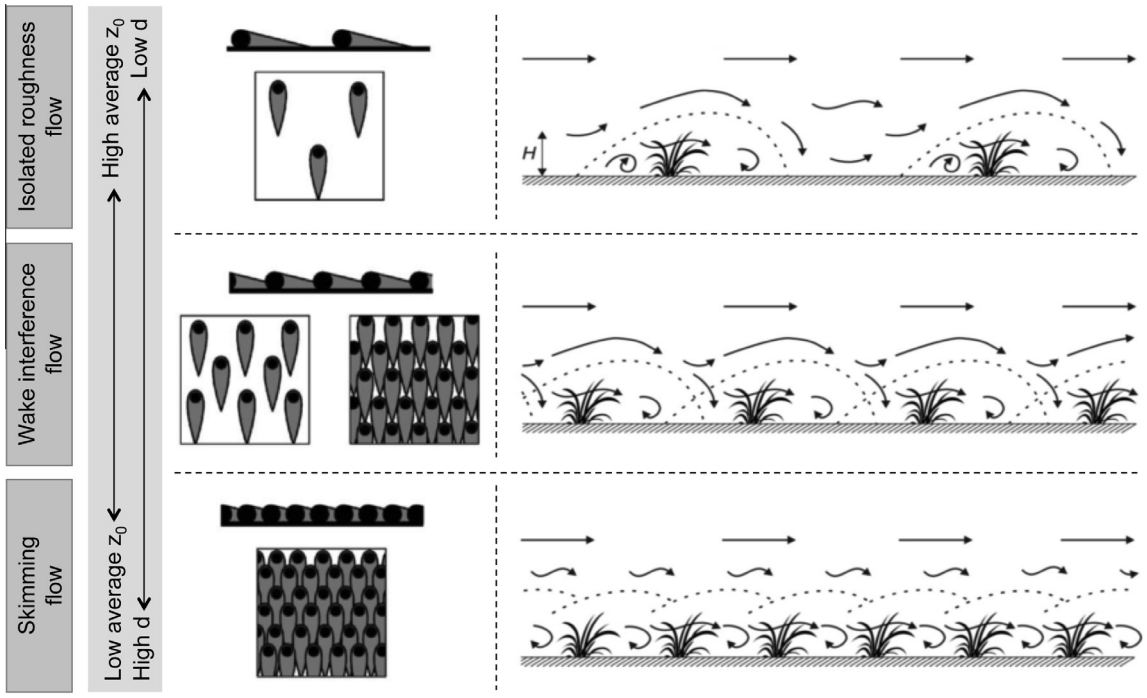

Fig. 1. Flow regimes and associated theoretical wake development, shown in schematic plan and side view. Shaded areas are wake regions. The effect of different flow regimes on average z_0 (aerodynamic roughness) and d (displacement height) per plant unit is shown (adapted from Wolfe and Nickling, 1993, p.57, and Suter-Burri et al., 2013, p. 66).

Whilst the Okin model shows good agreement with aeolian sand flux data at the plant/patch scale (Li et al., 2013; Sankey et al., 2013), its parameterisation of shear stress recovery downwind of a vegetated patch is based on two-dimensional wind fence and drag plate data from Bradley and Mulhearn (1983). In reality, two-dimensional fences represent a far simpler aerodynamic problem than three-dimensional live plants (Leenders et al., 2007), yet robust field data on the aerodynamic impact of vegetation patches is still lacking. Since changes to the distribution, geometry and scale of patches are thought to have significant effects on sediment transport and the evolution of dynamic vegetated landscapes (Okin and Gillette, 2001; Bergametti and Gillette, 2010; von Hardenberg et al., 2010; Sankey et al., 2012; Stewart et al., 2014), it is important to parameterise patch-induced skimming flow in models such as Okin's (2008) as accurately as possible.

This study aims to collect field-based, empirical data on the recovery of turbulent wind flow in the lee of a live, three-dimensional vegetation patch. Improved parameterisations of flow turbulence and sediment transport potential in vegetation patches in large-scale dryland landscape models are key for enhancing current understanding of how semi-vegetated desert surfaces might react to future environmental and anthropogenic changes.

2. Methods

2.1. Field site

The field study was carried out in the southwestern Kalahari Desert in Namibia (Fig. 2), ~4 km north of the Auob River (25°29′15″ S, 19°40′35″ E). The experimental site was located in a farmer's field on raised, flat terrain populated mainly by *Stipagrostis amabilis* grasses and *Rhigozum trichotomum* shrubs. The patch of vegetation chosen for this study was made up of dense grass and shrub cover separated from a non-vegetated area by a short, highly permeable wire fence. The vegetation patch on the upwind side was approximately 70 m × 70 m, with a mean surface cover of ~80%, a mean height of 1.10 m and a standard deviation of 0.11 m (large shrubs) and 0.08 m (grasses). Mean surface cover and height were assessed by recording the height and canopy width of each plant within nine 4 m^2 quadrats place at random locations within the patch. Heavy grazing on the downwind side of the cattle fence had resulted in a distinct patch of reduced vegetation cover, which was raked to clear any remaining nonerodible elements for the purposes of the experiment (Fig. 2b).

2.2. Experimental setup

Three 3D sonic anemometers (*Campbell CSAT-3*) were deployed at the study site to collect wind velocity data (u, horizontal; v, spanwise; and w, vertical) at a sampling frequency of 10 Hz. A mobile anemometer array (Fig. 2c) was erected with two sonic anemometers fixed onto a mobile steel mast to allow the array to be moved along a transect downwind of the patch edge, in two setups. In setup 1, the anemometers were mounted at heights of 0.30 m and 1.10 m. A height of 0.30 m corresponds to a balance between capturing turbulence that occurs close to the surface, whilst minimising the interference of saltating sand with the sonic measurement path (Weaver and Wiggs, 2011). A height of 1.10 m corresponds to the average element height (1 h) of the vegetation patch. In setup 2, the anemometers were erected at heights of 0.55 m and 1.65 m, representing 0.5 h and 1.5 h of the average patch height respectively. The downwind distance from the patch edge, in terms of average patch height, is referred to as 'h_d'. The mobile array was progressively moved downwind from the patch edge, such that wind velocity was recorded at all four heights at six locations: 1 h_d, 4 h_d, 7 h_d, 11 h_d, 15 h_d and 20 h_d.

A third anemometer was mounted at 1.40 m height (mean patch height + 0.30 m) and placed 8 h (8.80 m) upwind and 30 h (33.0 m) to the side of the measurement transect. By being located above the vegetation patch to capture the skimming flow at the same relative height as the near-surface measurements in the patch wake (i.e. 0.30 m height), this third anemometer provided reference wind data against which the mobile anemometry data could be normalised. Fig. 2d demonstrates that this reference reflected an undisturbed measurement of uniform flow over the patch. The anemometers were all aligned parallel with the prevailing wind direction and level in the horizontal plane. To ensure sufficient data were acquired for subsequent analysis, each setup was run for a minimum of 20 min.

2.3. Data analysis

Mean approach wind velocities as measured by the reference anemometer during each measurement setup ranged from 2.57 m s^{-1} to 3.70 m s^{-1}. In order to ensure that the airflow detected at each measurement location had interacted with roughly the same length of upwind patch (~70 m), the datasets were filtered to exclude approach wind directions >5° from the mean wind direction throughout the course of the experiment (cf. Mayaud et al., 2016). Following the application of the 5° threshold filter, the remaining datasets for each setup were 5.5–15.0 min long, which is in accordance with the recommendations of van Boxel et al. (2004) for capturing the full range of turbulent eddies to accurately represent boundary layer processes. Since Reynolds stress calculations are somewhat dependent on the interval length used, calculations from 5.5-min subsets of longer measurement runs were compared to those derived from the full run periods. Results did not vary by more than ±1.3%. All wind flow parameters were normalised by the appropriate measurement recorded simultaneously by the upwind reference anemometer at 1.40 m height. Normalisation is indicated using the '*norm*' subscript for each parameter.

The sonic anemometer data were post-processed to correct for any minor errors in aligning the anemometer heads into the mean approach wind flow. The streamwise frame of reference was rotated in accordance with the local streamline angle using yaw rotation (cf. van Boxel et al., 2004; Walker, 2005; Weaver and Wiggs, 2011; Chapman et al., 2012). Subsequent to yaw rotation correction the average spanwise velocity was zero ($\bar{V} = 0$), and so no further analysis of this component was undertaken. There is much discussion in the literature (e.g. Lee and Baas, 2012) about the necessity to correct for pitch in sonic anemometer datasets, which forces the average vertical velocity to zero ($\bar{W} = 0$). The purpose of this study is to characterise the behaviour of wind flow horizontal to the surface, rather than along the plane of the streamlines, so pitch rotation was omitted here. The application of roll rotation remains disputed practice for three-dimensional flow over non-uniform terrain (Kaimal and Finnigan, 1994; Lee and Baas, 2012), but the need for such a rotation is obviated by accounting for the spanwise flow component when calculating shear stress (see Eq. (1)).

The remaining velocity data were decomposed into their average ($\bar{U}, \bar{V}$ and $\bar{W}$) and fluctuating (u', v' and w') components, from which the horizontal ($\overline{u'^2}$) and vertical ($\overline{w'^2}$) components of Reynolds stress were derived. The resultant horizontal shear stress (τ_r), which is a more robust estimate of the total shearing force acting on the surface than the traditionally-employed Reynolds shear stress (τ, or $-\overline{u'w'}$), was calculated using both the streamwise and spanwise shear (Lee and Baas, 2012):

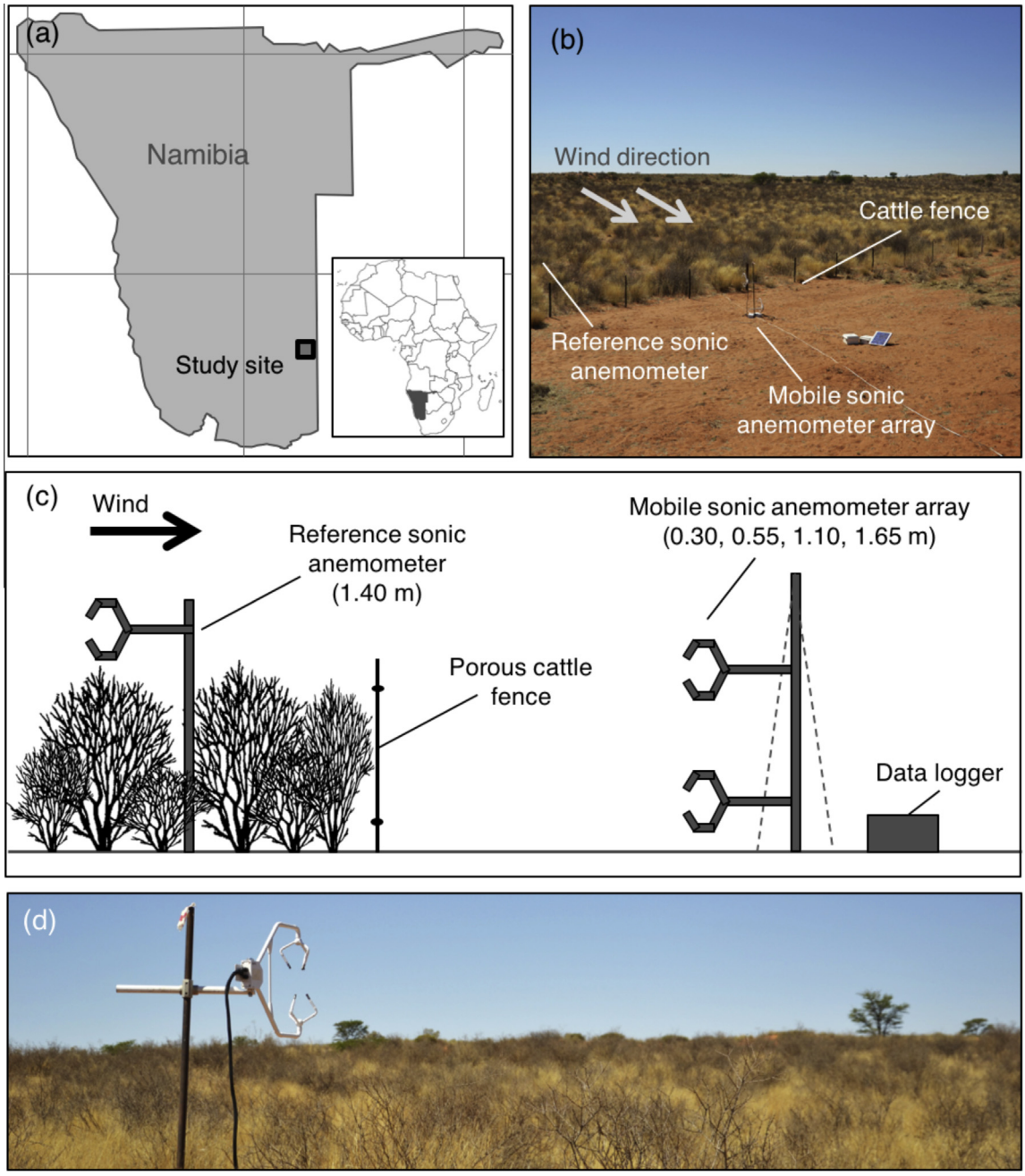

Fig. 2. (a) Location map of the field site in the southwestern Kalahari Desert; (b) photograph of the experimental setup downwind of the vegetation patch; (c) schematic diagram of the experimental setup (not to scale); (d) close-up of the reference anemometer.

$$\tau_r = \left(\overline{u'w'}^2 + \overline{v'w'}^2\right)^{1/2} \quad (1)$$

The local near-surface wind streamline angles along the wake transect were calculated as:

$$\theta = \arctan\left(\frac{\bar{W}}{\bar{U}}\right) \quad (2)$$

From these parameters, the incidence of coherent structures in the flow was established using conditional-sampling quadrant analysis (Lu and Willmarth, 1973). This technique defines four discrete categories of momentum exchange based on the relative signs of u' and w'. Ejections (Q2 events; $u' < 0$, $w' > 0$) and sweeps (Q4; $u' > 0$, $w' < 0$) contribute positively to the production of Reynolds stress, whilst outward interactions (Q1; $u' > 0$, $w' > 0$) and inward interactions (Q3; $u' < 0$, $w' < 0$) contribute negatively to Reynolds stress (Smith, 1996). In order to isolate significant bursts of turbulent stress from weaker background variability (Lapointe, 1992; Clifford and French, 1993), stress events of low magnitude were removed from quadrant analysis using a threshold criterion (H). Following previous studies (Bauer et al., 1998; Sterk et al., 1998; Leenders et al., 2005; Weaver, 2008; Wiggs and Weaver, 2012; Mayaud et al., 2016), the size of H was chosen to be equivalent to one standard deviation (σ) of the resultant horizontal shear stress (τ_r), such that a flow structure was only classified if $\tau_r > \pm H$. τ_r.

95% confidence intervals for the resultant horizontal shear stress (τ_{rCI}) and horizontal normal Reynolds stress ($\overline{u'^2}_{CI}$) were

established using the standard error of the mean around the relevant parameters (adapted from Lee and Baas, 2016):

$$\tau_{rCI} = 1.96\sqrt{\left(\frac{\sigma_{u'w'}}{\sqrt{N}}\right)^2 + \left(\frac{\sigma_{v'w'}}{\sqrt{N}}\right)^2} \quad (3)$$

$$\overline{u'^2}_{CI} = 1.96\sqrt{\left(\frac{\sigma_{u'^2}}{\sqrt{N}}\right)^2} \quad (4)$$

where N is the sample size. For normalised parameters, the total confidence interval for each data acquisition was calculated by summing the confidence intervals for both the local and reference shear stress parameters.

Shear velocity (u_*) can be related directly to the turbulent momentum flux (Walker, 2005; Lee and Baas, 2016):

$$u_* = (\overline{u'w'}^2 + \overline{v'w'}^2)^{1/4} \quad (5)$$

This relationship is important because it allows the aerodynamic roughness length (z_0) to be characterised using sonic anemometer datasets at single heights, without the need for a full velocity profile to be measured at multiple heights. The logarithmic profile for the inertial sublayer follows the 'Law of the Wall' (see King et al., 2005), which can be described by the Karman-Prandtl velocity distribution:

$$\frac{u_z}{u_*} = \frac{1}{\kappa}\ln\frac{z}{z_0} \quad (6)$$

where u_z is the mean wind speed at height z (m), and κ is the von Karman constant (dimensionless) equal to 0.4. By rearranging Eq. (6) and substituting τ_r for u_* (Eq. (5)), z_0 can be estimated directly from the resultant horizontal shear stress at a single height:

$$z_0 = \frac{z}{e^{\kappa\frac{u}{\sqrt{\tau_r}}}} \quad (7)$$

The Law of the Wall is only valid in cases where the internal boundary layer is in equilibrium with the surface roughness (King et al., 2005). Therefore, the analysis based on Eqs. (6) and (7) is only applied to data collected above the vegetation patch (where the skimming flow is considered in equilibrium with the patch roughness), and sufficiently far downwind of the reattachment point in the lee of the patch, where the internal boundary layer has grown in equilibrium with the desert surface.

In summary, our sonic anemometer data were employed to calculate variations in mean wind velocity, turbulent stresses, and coherent structures above and downwind of the vegetation patch. Mean wind velocity changes allow simple interpretations of wind flow recovery to be made, whilst turbulence parameters and coherent structures provide a more detailed picture of how the airflow structure varies at different points along the flow trajectory. In conjunction with aerodynamic roughness calculations made in zones where flow has equilibrated, these turbulence data can be used to identify the growth of an internal boundary layer, which has previously been shown to develop downwind of a step-change in roughness.

3. Results

3.1. Mean wind velocity

Fig. 3 displays the spatial patterns of mean normalised wind velocity (Φ) downwind of the patch. Normalised wind velocities at each measurement location were interpolated using a triangulation-based natural neighbour algorithm, with a grid spacing of 0.1 m. The algorithm was chosen because it produced realistic spatial features that were present using several other commonly used interpolation algorithms, and without obvious artefacts. Since the reference anemometer was placed at 1.40 m height, normalised velocities are expected to stabilise below $\Phi = 1.0$ at the lowest measurement heights in the patch wake.

The contour plot (Fig. 3a) shows a distinct region of lower wind velocity ($\Phi < 1.0$) near the surface (<~0.7 h) until ~6 h_d. At average patch height (i.e. 1 h) and above, there was a region of lower wind velocity from 0 to 12 h_d, followed by a marked zone of increased velocity ($\Phi > 1.0$) from 14 to 20 h_d. These differences relative to the reference anemometer likely result from the expansion of the wind flow into the gap in the lee of the patch, and from the different roughness represented by the patch compared to the bare surface in its wake; these points are explored further in relation to Fig. 4. The semi-logarithmic vertical profiles of Φ at each measurement location (Fig. 3b) were noticeably kinked up to a distance of 15 h_d, suggesting that airflow was disrupted, with a large amount of retardation near the surface, to at least this distance downwind of the patch edge.

Fig. 4 displays the best-fit normalised mean wind velocity curves (Φ) in the patch wake. The data at the four measurement heights were fitted using a saturating exponential function because this generally describes the recovery of wind flow downwind of an obstruction (Bradley and Mulhearn, 1983). Also presented is the recovery rate published by Okin (2008, corrected in Li et al., 2013) for parameterising surface shear stress downwind of a plant, based on the wind fence and drag plate data of Bradley and Mulhearn (1983).

The curves at 0.30 m and 0.55 m height were similar in shape, recovering to ~90% of their exponential saturation values (deemed to represent effective flow recovery; Okin, 2008) at 12–13 h_d. In comparison, Okin's (2008) curve recovers more quickly at ~10 h_d, and reported windflow recovery distances downwind of solitary elements are between 7 and 9 h_d (Leenders et al., 2007; Gillies et al., 2014; Wu et al., 2015; Mayaud et al., 2016). The recovery curves at 1.10 m and 1.65 m height were much shallower than at 0.30 m and 0.55 m height due to a smaller initial leeside reduction in wind velocity.

3.2. Turbulent stresses

Fig. 5 displays variations in normalised resultant horizontal shear stress (τ_{rnorm}), normalised horizontal normal Reynolds stress ($\overline{u'^2_{norm}}$) and streamline angle variations from the horizontal plane, downwind of the patch edge. Vertical velocity variations were roughly an order of magnitude smaller than the horizontal components of flow in this study (cf. Sterk et al., 1998; van Boxel et al., 2004; Leenders et al., 2005; Weaver and Wiggs, 2011; Mayaud et al., 2016), so play only a very minor role in flow dynamics. Vertical normal Reynolds stress ($\overline{w'^2}$) data are therefore not presented here.

Values of τ_{rnorm} (Fig. 5a) were generally highest in the immediate lee of the patch, particularly at greater measurement heights, and decreased with increasing downwind distance. Stress curves at all heights converged further downwind, starting with the curves at the two lowest heights around 15 h_d, and progressive convergence at greater heights. This indicates the progressive equilibration of the new internal boundary layer forming in response to the smoother desert surface (Belcher et al., 2003). A constant stress layer was observed at 20 h_d, corresponding to the equilibrating semi-logarithmic vertical profiles of Φ shown Fig. 3b. This constant stress layer displayed lower shear stress values than the constant stress layer above the vegetation patch (i.e. $\tau_{rnorm} < 1$) due to the lower surface roughness of the bare sand surface compared to the vegetation. The impact of the changing surface roughness on wind flow was also evident from shear velocity (u_*) calculations

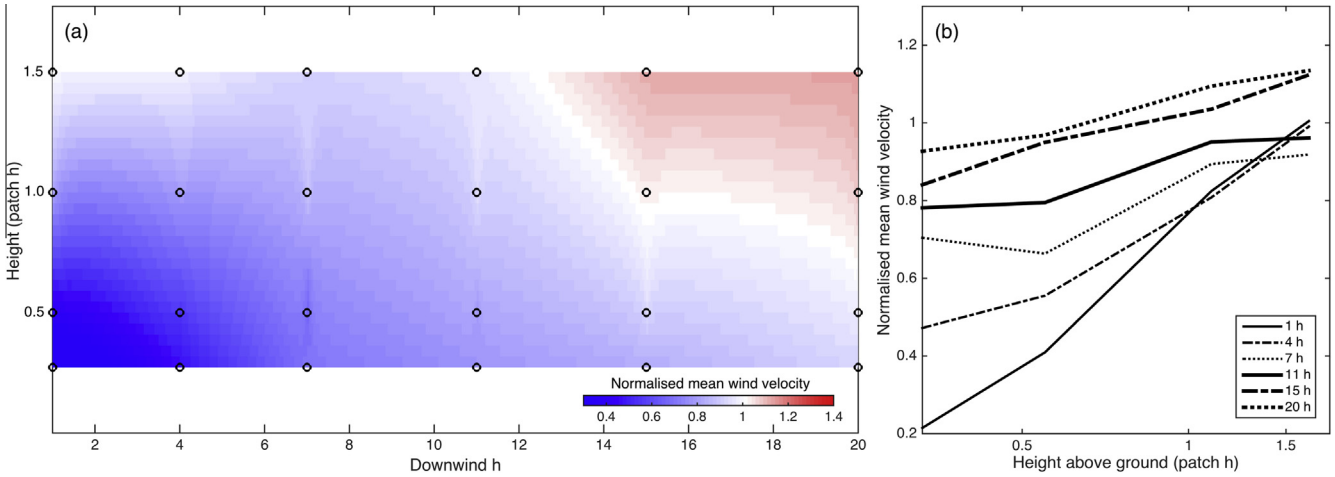

Fig. 3. (a) Contour plot of normalised mean wind velocity (Φ) at all measurement locations (in terms of patch height, h) downwind of the patch. Black circles represent anemometer locations; (b) Vertical profile of Φ at the six measurement locations along the wake transect (note that x axis is logarithmic).

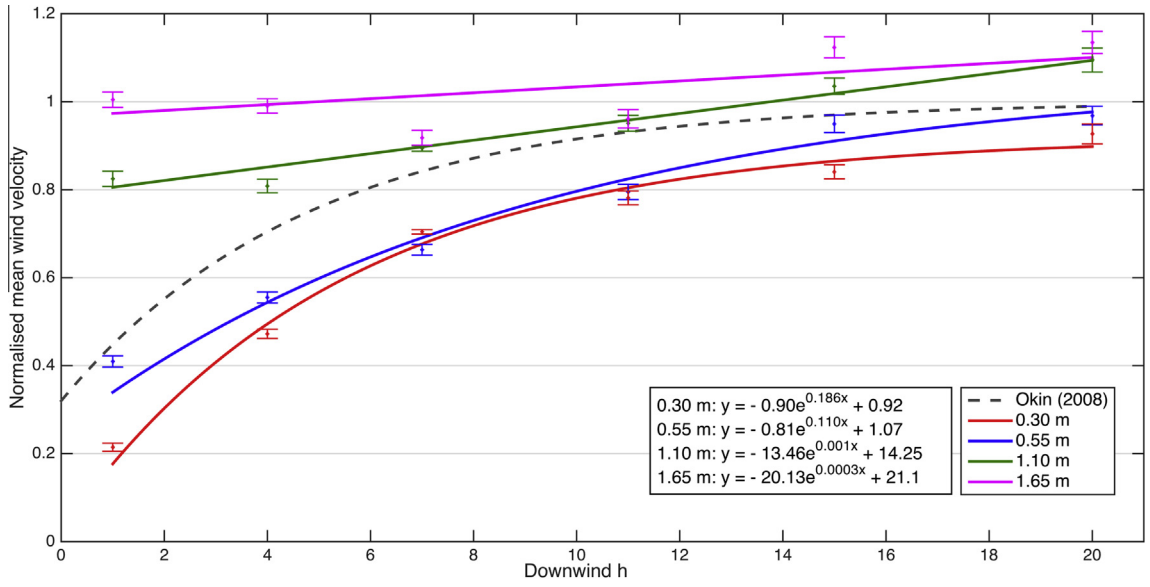

Fig. 4. Best fit regression lines for normalised mean wind velocity (Φ) at all measurement heights (0.30 m, 0.55 m, 1.10 m and 1.65 m) downwind of the patch. Error bars represent the standard deviation of the mean. Also shown is Okin's (2008; corrected in Li et al., 2013) parameterisation of reduced shear stress downwind of a plant. Table displays function form for the general fitting models at each measurement height.

(Eq. (5)), with $u_* = 0.46$ m s^{-1} above the vegetation patch (corresponding to an aerodynamic roughness (z_0) of 0.022 m), and $u_* = 0.24$ m s^{-1} ($z_0 = 0.001$ m) at 20 h_d. In contrast to $-\overline{u'w'}_{norm}$, values of $\overline{u'^2}_{norm}$ (Fig. 5b) were lowest in the immediate lee of the patch and increased at greater downwind distances, broadly following the pattern of normalised wind velocity.

The change in airflow structure resulting from the patch/bare surface transition can also be observed in the streamline angles of the flow (Fig. 5c). Streamline angles were negative (i.e. the flow was angled towards the surface as the air expanded into the void in the lee of the patch) in the immediate lee of the patch until at least 4 h_d. At 1 h_d at 0.30 m height, horizontal wind flow was negative for 11.2% of the time, implying that the downward movement of air occasionally translated into bursts of flow moving back towards the patch, whereas at all other measurement locations (including the above-patch reference anemometer) horizontal wind flow was negative <0.01% of the time. Whilst this does not imply the formation of a full recirculation zone, the low wind velocities in the immediate lee of the patch likely create a zone of semi-recirculation near the base of the vegetation (e.g. Hagen and Skidmore, 1971; Cornelis and Gabriels, 2005; Sutton and McKenna-Neuman, 2008; Lee et al., 2014). From 7 to 15 h_d, streamline angles increased to ~3°, likely resulting from the deflection of downward-moving wind as the flow reattached to the surface.

Whilst shear stress and streamline angle variation in the airflow is useful to some extent in characterising wind flow (see Section 4), previous aeolian studies have highlighted the significance of the coherency, or structured nature, of turbulence in the context of plant canopies (e.g. Shaw et al., 1983; Yue et al., 2007) and dunes (e.g. van Boxel et al., 2004; Leenders et al., 2005; Chapman et al., 2012, 2013; Wiggs and Weaver, 2012). In order to segregate the stress budget between different structures in the flow in the patch wake, quadrant analysis (Lu and Willmarth, 1973; see Section 2.3) was conducted.

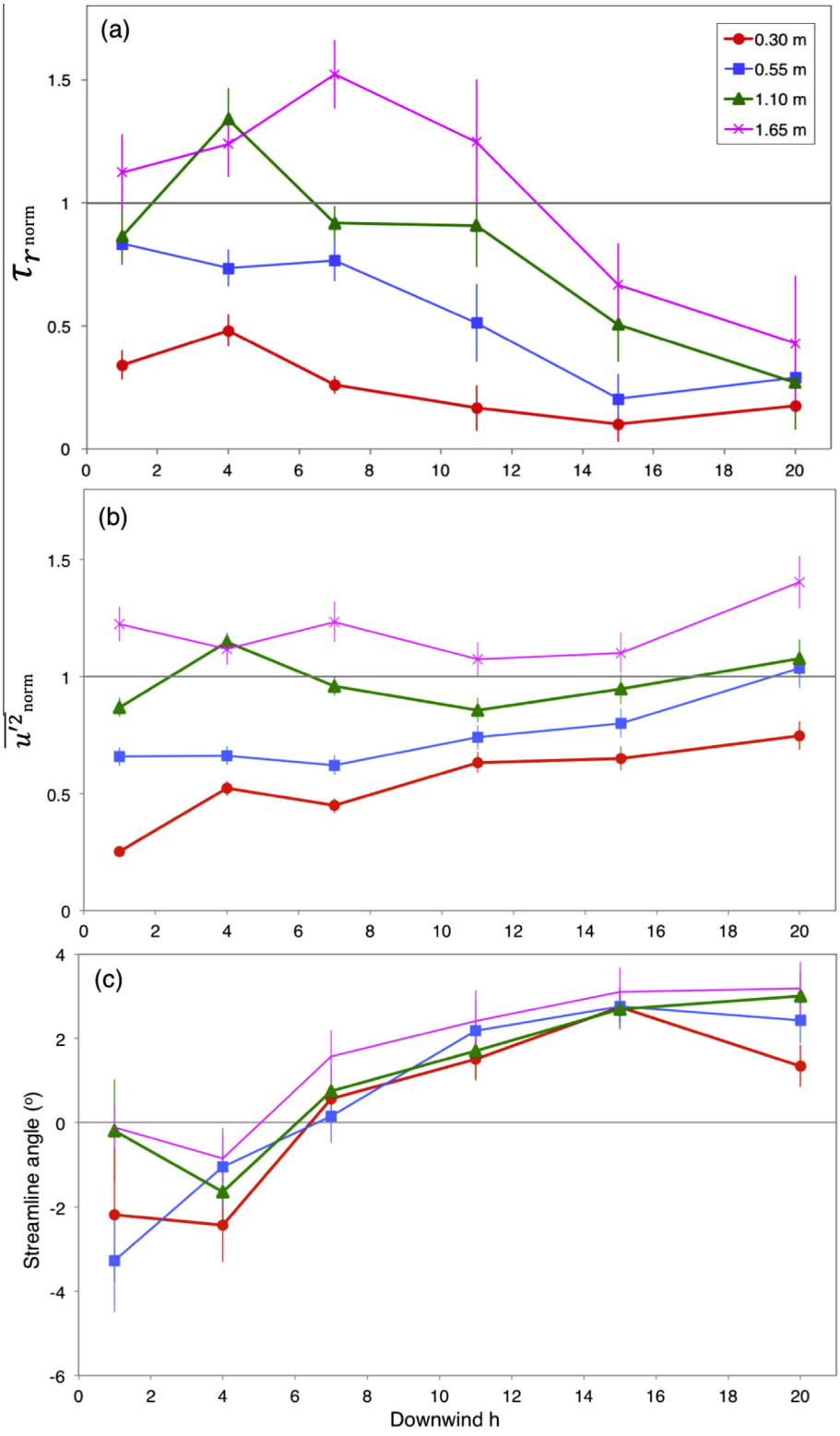

Fig. 5. Variations in turbulence parameters downwind of the patch, at the four measurement heights: (a) normalised resultant horizontal shear stress ($\tau_{r,norm}$); (b) horizontal normal Reynolds stress ($\overline{u'^2}_{norm}$); (c) streamline angle variation from the horizontal plane. Confidence intervals at the 95% level are shown as vertical bars.

3.3. Coherent flow structures

Fig. 6 displays the frequency of occurrence of coherent structures (quadrant events) along the patch wake at the four measurement heights. There was a sharp increase in the frequency of Q4 (sweep) events in the immediate lee of the patch, particularly nearer the surface, where Q4 events constituted up to 61.8% of the flow. From 0.55 m to 1.65 m height, there was a high frequency of Q2 (ejection) events in the immediate lee. Q2 and Q4 events were also very prevalent above the patch canopy. The dominance of Q2 and Q4 events progressively decreased with greater downwind distance, and Q1 and Q3 event frequencies increased from

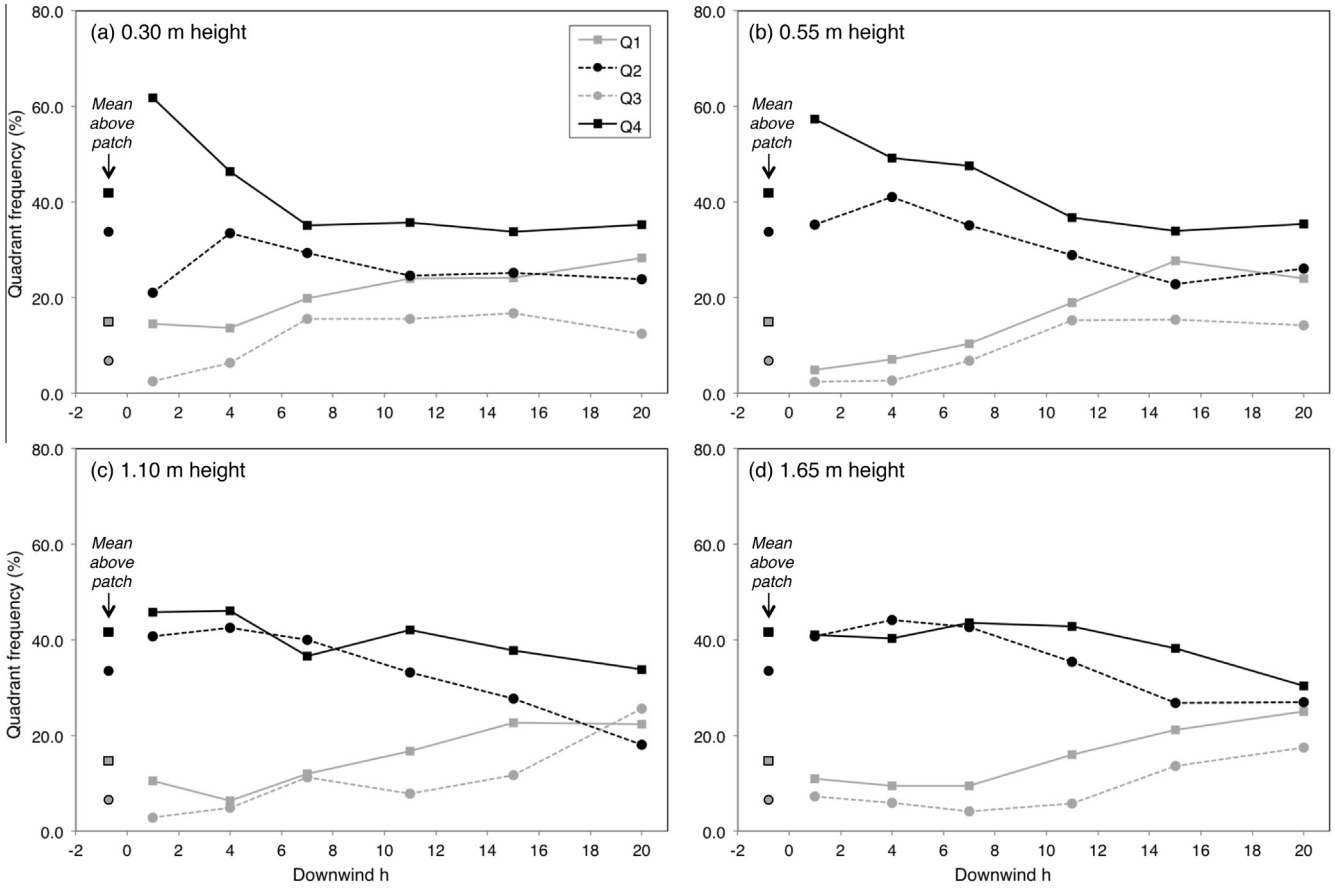

Fig. 6. Frequency of occurrence (%) of coherent structures along the patch wake, at the four measurement heights: Q1 = outward interaction ($u' > 0$, $w' > 0$), Q2 = ejection ($u' < 0$, $w' > 0$), Q3 = inward interaction ($u' < 0$, $w' < 0$), Q4 = sweep ($u' > 0$, $w' < 0$). Mean quadrant values above the patch are also shown for reference.

Table 1
Quadrant frequencies in unperturbed flow over bare, flat surfaces, as reported in previous studies.

Study	Measurement height (m)	Quadrant frequency range (%)			
		Q1	Q2	Q3	Q4
Mayaud et al. (2016)	0.30	19–26	31–39	8–16	33–37
Weaver (2008)	0.30	19–22	31–33	16–19	29–32
	1.50	19–23	32–36	18–22	22–27
Leenders et al. (2005)	2.0	23–27	22–33	11–18	33–36

<15% in the immediate lee to reach 15–30% at most heights around 15–20 h_d. The equilibration of flow was evident from the stabilisation of all quadrant curves by 20 h_d, supporting evidence from the measure variations in τ_r (Fig. 5). The quadrant frequencies at 20 h_d in this study are similar to previously reported quadrant frequencies in unperturbed flow over bare, flat surfaces (see Table 1).

4. Discussion

A distinct near-surface region of lower wind velocity ($\Phi < 1.0$) was detected at several heights in the wake of our study patch (Figs. 3 and 4). The longer recovery length downwind of the patch (~12 h_d) compared with isolated elements of equivalent height reported in other studies (7–9 h_d; Leenders et al., 2007; Gillies et al., 2014; Wu et al., 2015; Mayaud et al., 2016) can be attributed to a lack of flow moving around the patch. In contrast, isolated elements divert wind flow around their sides, leading to faster-moving airflow that mixes with slower-moving flow in their wakes via counter-rotating vortices and leads to more rapid recovery (Sutton and McKenna-Neuman, 2008). In a numerical modelling study designed to simulate airflow around forest edges, Liu et al. (1996) also found that the effect of a forest patch on mean wind velocity could be detected relatively far downwind, up to 22 h_d. Okin's (2008) recovery curve is based on data from a two-dimensional wind fence experiment where the change in roughness was not sufficient to engender skimming flow, so the more significant alteration to flow equilibrium in the patch case examined in this study understandably results in a longer recovery than Okin's curve. This could imply that the potential for sediment transport downwind of a skimming flow regime is reduced compared to isolated roughness and wake interference flow regimes.

The recovery curves at greater heights (1.10 m and 1.65 m) were much shallower than at the surface due to a smaller initial leeside reduction in wind velocity. Flow above the patch was retarded relative to the bare surface due to the higher roughness value of the vegetation, which resulted in wind velocities at average vegetation height (z = 1.10 m) increasing in relative terms downwind of the patch. The observed slowdown in wind velocity at 1.65 m height likely resulted from the static pressure at the downwind edge of the patch increasing as a response to airflow expanding into the un-vegetated zone below, as well as from the difference in roughness (Belcher et al., 2003) represented by the patch (z_0 = 0.022 m) compared to the bare surface in its wake (z_0 = 0.001 m at 20 h_d).

It should be noted that the range of mean reference wind velocities recorded during this study was relatively narrow (2.57–3.70 m s^{-1}). Several windbreak studies (e.g. Hagen and Skidmore, 1971; Wu et al., 2015) have shown that free stream velocity affects

windbreak performance. In wind tunnel experiments conducted over a range of wind velocities (5–12.5 m s^{-1} at an equivalent real-world height of 10 m), Wu et al. (2015) showed that the zone of reduced velocity in the immediate lee of a windbreak expands by up to 3 h_d (thus leading to a decreased recovery rate) as the free-stream velocity increases. Using wind data at 20 h_d of our study patch, where the airflow was broadly in equilibrium with the bare surface, the wind shear velocity ($u_* = 0.24$ m s^{-1}) and the aerodynamic roughness ($z_0 = 0.001$ m), Law of the Wall assumptions suggest that wind velocities at 10 m height (cf. Hagen and Skidmore, 1971; Wu et al., 2015) were ~5.5 m s^{-1} during our experiment. This value is at the lower end of Wu et al.'s (2015) experimental conditions, which could mean that airflow recovery observed in the wake of our study patch may differ slightly at higher wind velocities. However, since the non-uniform turbulent flows measured in this study likely have high Reynolds numbers, an increase in wind velocity is unlikely to result in major changes to the wake structure.

Alongside characterising mean wind velocity, the impact of vegetation on driving flow turbulence must also be considered. High shear stresses observed at multiple heights in the immediate lee of the patch (Fig. 5a) were likely a result of airflow at the surface accelerating in response to the lack of vegetation and skimming flow expanding into the leeside void, leading to a growth of an internal boundary layer (Greeley and Iversen, 1985; Wiggs et al., 1994, 1996). The change in wind structure was evident from the kinked profiles in Fig. 3b, as the flow re-equilibrated to the new roughness. Flow above the mean patch height (>1.10 m height) was still responding to the quasi-stable above-canopy drag induced by the vegetation (Belcher et al., 2003; Tischmacher and Ruck, 2013), up until 4–7 h_d. Nearer the surface, the rapidly declining shear stress indicated a separation of the upper shear layer, as previously reported above porous wind fences (e.g. Kim and Lee, 2002). Further downwind, the convergence of stress curves at all heights and the decline in aerodynamic roughness length suggests that the new internal boundary layer forming in response to the smoother surface was progressively equilibrating. The z_0 measured at 20 h_d of our study patch (~0.001 m) was very similar to that measured by Wiggs et al. (1994) above a bare, burnt surface in the Kalahari (0.002–0.003 m). Above the study patch, our calculated z_0 (0.022 m) was roughly an order of magnitude lower than Wiggs et al.'s (1994) calculated z_0 (0.2 m) above a vegetated surface (z = 0.8–1.0 m), most likely because flow at their vegetated site had not developed into skimming flow.

The changing distributions of quadrant events (Fig. 6) along the measurement transect provide context for the Reynolds stress patterns identified in Fig. 5. The high prevalence of Q2 and Q4 events in the lee contributed positively to τ_r calculations, and thus account for the peak in τ_r in this region (Fig. 5a). Meanwhile, the increasing occurrence of Q1 events downwind can be linked to the observed increase in $\overline{u'^2}$ along the wake (Fig. 5b), since outward interactions are partly defined as positive deviations away from mean horizontal flow. The relative changes in turbulent structure proportions resulting from the presence of vegetation are important to quantify, because of the role they are understood to play in driving sediment transport. In the fluvial domain, a turbulent 'bursting process' (relatively greater occurrence of Q2 and Q4 events), has been shown to be a key determinant of transport (Best and Kostaschuk, 2002), but there is evidence that aeolian sediment transport is better associated with turbulent structures characterised by a positive streamwise fluctuating velocity ($u' > 0$, Q1 and Q4 events) (e.g. Sterk et al., 1998; Schönfeldt and von Löwis, 2003; van Boxel et al., 2004; Wiggs and Weaver, 2012; Chapman et al., 2013). This is why the $\overline{u'^2}$ parameter, which directly accounts for streamwise variability, is often better correlated with sediment transport than Reynolds shear stress (Wiggs and Weaver, 2012). The difference between aeolian and fluvial turbulent processes driving sediment transport is likely to be due to the greater disparity in density ratio between sand particles and wind compared with water (Wiggs and Weaver, 2012).

Whilst no direct links can be made between horizontal turbulence and sediment transport in this study, there is increasing evidence that some turbulent stresses are important driving forces for aeolian sediment entrainment and transport in complex flows (Butterfield, 1991; Sterk et al., 1998; Schönfeldt and von Löwis, 2003; Leenders et al., 2005, 2007; Baddock et al., 2011; Weaver and Wiggs, 2011; Wiggs and Weaver, 2012; Chapman et al., 2012, 2013). Given that the wind flow in the immediate lee of the patch did not exist as a well-developed equilibrium boundary layer, it is not possible to interpret the sediment transport potential in this zone (Schlichting, 1955). It has been argued that only the shear stress measured directly at the surface (e.g. using Irwin sensors) can provide information on erosion potential in non-equilibrium conditions (Walter et al., 2012). However, as the flow equilibrated downwind of the reattachment point, the relative increases in Q1 events, wind velocities and $\overline{u'^2}$ suggest that sediment transport could develop downwind of the flow recovery zone.

5. Conclusion

Results from this study show that in the wake of a vegetation patch that is extensive and dense enough to produce skimming flow, wind velocity effectively recovers by ~12 h_d. This is 2–5 h longer than previously reported recovery distances for individual vegetation elements and two-dimensional wind fences (e.g. Raupach, 1992; Minvielle et al., 2003; Leenders et al., 2007; Okin, 2008; Gillies et al., 2014; Mayaud et al., 2016), which can be attributed to a lack of faster flow moving around the obstacle in the patch case.

The use of τ_r measurements at multiple heights was shown to be a useful tool for characterising airflow structure across the patch/bare surface transition. The step-change in roughness between the patch canopy and the bare surface, evident from the difference in aerodynamic roughness (z_0) above the patch ($z_0 = 0.022$ m) compared to 20 h_d ($z_0 = 0.001$ m), caused an initial peak in resultant horizontal shear stress (τ_r) as the skimming flow expanded into the leeside void, followed by a large reduction in τ_r as a new internal boundary layer grew. The convergence of τ_r across all measurement heights implied the formation of a constant stress layer (i.e. equilibration) by 20 h_d.

Quadrant analysis identified elevated frequencies of Q2 (ejection) and Q4 (sweep) events in the immediate lee of the patch, which accounts for high τ_r in this region and a potential enhancement to the 'bursting process' in the lee. Whilst it is not possible to directly link the turbulent wind flow parameters reported in this study to sediment transport, the increasing contribution of Q1 (outward interaction) events along the patch wake, coinciding with increasing $\overline{u'^2}$ and wind velocity, suggests that sediment transport potential most likely increases with greater distance from the patch edge.

By providing the first field-based dataset of wind flow in the wake of a real vegetation patch, this research builds on existing parameterisations to better constrain the effects of vegetation on turbulent wind dynamics. Since shifts in vegetation structure relating from environmental and anthropogenic stresses such as grazing, fire and climatic change could significantly impact sediment mobility in semi-arid regions (Okin and Gillette, 2001; Sankey et al., 2012), it is vital to improve our understanding of

the aerodynamic behaviour of patchy vegetation. The new data presented here can be integrated into wind erosion and landscape evolution models, in order to better understand the potential response of semi-vegetated surfaces to future environmental and anthropogenic stresses.

Acknowledgements

This research was funded by a UK Natural Environment Research Council Doctoral Training Grant (NE/L501530/1), a St Catherine's College (Oxford) Scholarship and a Hertford College (Oxford) Scholarship to J.R.M. We thank P. and H. Möller for their kind permission to conduct fieldwork on their land. Two reviewers are thanked for their constructive comments that helped to improve this paper.

References

Al-Awadhi, J.M., Willetts, B.B., 1999. Sand transport and deposition within arrays of non-erodible cylindrical elements. Earth Surf. Proc. Land. 24, 423–435.
Ash, J.E., Wasson, R.H., 1983. Vegetation and sand mobility in the Australian desert dunefield. Zeitschrift für Geomorphologie [Suppl.] 45, 7–25.
Baas, A.C.W., Sherman, D.J., 2005. Formation and behaviour of aeolian streamers. J. Geophys. Res. 110, F03011.
Baddock, M.C., Wiggs, G.F.S., Livingstone, I., 2011. A field study of mean and turbulent flow characteristics upwind, over and downwind of barchan dunes. Earth Surf. Proc. Land. 36 (11), 1435–1448. http://dx.doi.org/10.1002/esp.2161.
Bailey, R.M., 2011. Spatial and temporal signatures of fragility and threshold proximity in modelled semi-arid vegetation. Proc. R. Soc. B 278, 1064–1071.
Bauer, B.O., Yi, J., Namikas, S.L., Sherman, D.J., 1998. Event detection and conditional averaging in unsteady aeolian systems. J. Arid Environ. 39, 345–375.
Belcher, S., Jerram, N., Hunt, J., 2003. Adjustment of a turbulent boundary layer to a "canopy" of roughness elements. J. Fluid Mech. 488 (1), 369–398. http://dx.doi.org/10.1017/S0022112003005019.
Bergametti, G., Gillette, D.A., 2010. Aeolian sediment fluxes measured over various plant/soil complexes in the Chihuahuan desert. J. Geophys. Res. 155, F03044.
Best, J.L., Kostaschuk, R.A., 2002. An experimental study of turbulent flow over a low-angle dune. J. Geophys. Res. 107 (C9), 3135. http://dx.doi.org/10.1029/2000JC000294.
Bradley, E.F., Mulhearn, P.J., 1983. Development of velocity and shear-stress distributions in the wake of a porous shelter fence. J. Wind Eng. Ind. Aerodyn. 15 (1–3), 145–156.
Breshears, D.D., Whicker, J.J., Zou, C.B., Field, J.P., Allen, C.D., 2009. A conceptual framework for dryland aeolian sediment transport along the grassland–forest continuum: effects of woody plant canopy cover and disturbance. Geomorphology 105, 28–38.
Burri, K., Gromke, C., Lehning, M., Graf, F., 2011. Aeolian sediment transport over vegetation canopies: a wind tunnel study with live plants. Aeolian Res. 3, 205–213.
Butterfield, G.R., 1991. Grain transport rates in steady and unsteady turbulent airflows. Acta Mechanica (Suppl.) 1, 97–122.
Chapman, C.A., Walker, I.J., Hesp, P.A., Bauer, B.O., Davidson-Arnott, R.G.D., 2012. Turbulent Reynolds stress and quadrant event activity in wind flow over a coastal foredune. Geomorphology 151–152, 1–12.
Chapman, C., Walker, I.J., Hesp, P.A., Bauer, B.O., Davidson-Arnott, R.G.D., Ollerhead, J., 2013. Reynolds stress and sand transport over a foredune. Earth Surf. Proc. Land. 38 (14), 1735–1747.
Clifford, N.J., French, J.R., 1993. Monitoring and modelling turbulent flows: historical and contemporary perspectives. In: Clifford, N.J., French, J.R., Hardisty, J. (Eds.), Turbulence: Perspectives on Flow and Sediment Transport. John Wiley & Sons, New York, pp. 1–34.
Cornelis, W.M., Gabriels, D., 2005. Optimal windbreak design for wind-erosion control. J. Arid Environ. 61 (2), 315–332.
Crawley, D.M., Nickling, W.G., 2003. Drag partition for regularly-arrayed rough surfaces. Bound. Layer Meteorol. 107, 445–468.
Davidson-Arnott, R.G.D., Bauer, B.O., Walker, I.J., Hesp, P.A., Ollerhead, J., Chapman, C., 2012. High-frequency sediment transport responses on a vegetated foredune. Earth Surf. Proc. Land. 37 (11), 1227–1241.
Dupont, S., Bergametti, G., Simoëns, S., 2014. Modeling aeolian erosion in presence of vegetation. J. Geophys. Res.: Earth Surf. 119 (2), 168–187. http://dx.doi.org/10.1002/2013JF002875.
Frank, C., Ruck, B., 2008. Numerical study of the airflow over forest clearings. Forestry 81 (3), 259–277. http://dx.doi.org/10.1093/forestry/cpn031.
Gash, J.H.C., 1986. Observations of turbulence downwind of a forest-heath interface. Bound. Layer Meteorol. 36, 227–237.
Getzin, S., Wiegand, K., Wiegand, T., Yizhaq, H., von Hardenberg, J., Meron, E., 2014. Adopting a spatially explicit perspective to study the mysterious fairy circles of Namibia. Ecography. http://dx.doi.org/10.1111/ecog.00911.
Gillette, D.A., Stockton, P.A., 1989. The effects of non-erodible particles on wind erosion of erodible surfaces. J. Geophys. Res. 94 (D10), 12885–12893.
Gillette, D.A., Herrick, J.E., Herbert, G.A., 2006. Wind characteristics of Mesquite Streets in the northern Chihuahuan Desert, New Mexico, USA. Environ. Fluid Mech. 6 (3), 241–275.
Gillies, J.A., Lancaster, N., Nickling, W.G., Crawley, D., 2000. Field determination of drag forces and shear stress partitioning effects for a desert shrub (*Sarcobatus vermiculatus*, Greasewood). J. Geophys. Res.: Atmos. 105 (D20), 24871–24880.
Gillies, J.A., Nickling, W.G., King, J., 2002. Drag coefficient and plant form-response to wind speed in three plant species: burning bush (Euonymus alatus), Colorado blue spruce (Picea pungens glauca.), and fountain grass (Pennisetum setaceum). J. Geophys. Res. 107 (D24), 4760.
Gillies, J.A., Nield, J.M., Nickling, W.G., 2014. Wind speed and sediment transport recovery in the lee of a vegetated and denuded nebkha within a nebkha dune field. Aeolian Res. 12, 135–141.
Greeley, R., Iversen, J.D., 1985. Wind as a Geomorphological Process. Cambridge University Press, Cambridge.
Hagen, L.J., Skidmore, E.L., 1971. Turbulent velocity fluctuations and vertical flow as affected by windbreak porosity. Trans. Am. Soc. Agric. Eng. 14, 634–637.
Judd, M.J., Raupach, M.R., Finnigan, J.J., 1996. A wind tunnel study of turbulent flow around single and multiple windbreaks. Part I: velocity fields. Bound. Layer Meteorol. 80, 127–165.
Kaimal, J.C., Finnigan, J., 1994. Atmospheric Boundary Layer Flows: Their Structure and Measurement. Oxford University Press, New York.
Kim, H.B., Lee, S.-J., 2002. The structure of turbulent shear flow around a two-dimensional porous fence having a bottom gap. J. Fluids Struct. 16 (3), 317–329.
King, J., Nickling, W.G., Gillies, J.A., 2005. Representation of vegetation and other non-erodible elements in aeolian shear stress partitioning models for predicting transport threshold. J. Geophys. Res. 110, F04015.
Lapointe, M.F., 1992. Burst-like sediment suspension events in a sand bed river. Earth Surf. Proc. Land. 17, 253–270.
Le, H., Moin, P., Kim, J., 1997. Direct numerical simulation of turbulent flow over a backward-facing step. J. Fluid Mech. 330, 349–374.
Lee, Z.S., Baas, A.C.W., 2012. Streamline correction for the analysis of boundary layer turbulence. Geomorphology 171–172, 69–82. http://dx.doi.org/10.1016/j.geomorph.2012.05.005.
Lee, Z.S., Baas, A.C.W., 2016. Variable and conflicting shear stress estimates inside a boundary layer with sediment transport. Earth Surf. Proc. Land. 41 (4), 435–445. http://dx.doi.org/10.1002/esp.3829.
Lee, J.-P., Lee, E.-J., Lee, S.-J., 2014. Shelter effect of a fir tree with different porosities. J. Mech. Sci. Technol. 28 (2), 565–572. http://dx.doi.org/10.1007/s12206-013-1123-6.
Leenders, J.K., van Boxel, J.H., Sterk, G., 2005. Wind forces and related saltation transport. Geomorphology 71, 357–372.
Leenders, J.K., van Boxel, J.H., Sterk, G., 2007. The effect of single vegetation elements on wind speed and sediment transport in the Sahelian zone of Burkina Faso. Earth Surf. Proc. Land. 1454–1474. http://dx.doi.org/10.1002/esp.
Li, J., Okin, G.S., Alvarez, L., Epstein, H., 2008. Effects of wind erosion on the spatial heterogeneity of soil nutrients in two desert grassland communities. Biogeochemistry 88, 73–88.
Li, J., Okin, G.S., Herrick, J.E., Belnap, J., Miller, M.E., Vest, K., Draut, A.E., 2013. Evaluation of a new model of aeolian transport in the presence of vegetation. J. Geophys. Res.: Earth Surf. 118 (1), 288–306.
Liu, J., Chen, J.M., Black, T.A., Novak, M.D., 1996. E-ε modelling of turbulent air flow downwind of a model forest edge. Bound. Layer Meteorol. 77, 21–44.
Lu, S.S., Willmarth, W.W., 1973. Measurements of the structure of the Reynolds stress in a turbulent boundary layer. J. Fluid Mech. 60, 481–511.
Mayaud, J.R., Wiggs, G.F.S., Bailey, R., 2016. Characterising turbulent wind flow around dryland vegetation. Earth Surf. Proc. Land. http://dx.doi.org/10.1002/esp.3934.
Meron, E., Gilad, E., von Hardenberg, J., Shachak, M., Zarmi, Y., 2004. Vegetation patterns along a rainfall gradient. Chaos, Solitons Fractals 19 (2), 367–376.
Minvielle, F., Marticorena, B., Gillette, D.A., Lawson, R.E., Thompson, R., Bergametti, G., 2003. Relationship between the aerodynamic roughness length and the roughness density in cases of low roughness density. Environ. Fluid Mech. 3, 249–267.
Namikas, S.L., Bauer, B.O., Sherman, D.J., 2003. Influence of averaging interval on shear velocity estimates for aeolian transport modelling. Geomorphology 53 (3–4), 235–246.
Okin, G.S., 2008. A new model of wind erosion in the presence of vegetation. J. Geophys. Res. 113 (F2), F02S10.
Okin, G.S., Gillette, D.A., 2001. Distribution of vegetation in wind-dominated landscapes: implications for wind erosion modeling and landscape processes. J. Geophys. Res. 106, 9673–9683.
Okin, G.S., Gillette, D.A., Herrick, J.E., 2006. Multi-scale controls on and consequences of aeolian processes in landscape change in arid and semi-arid environments. J. Arid Environ. 65 (2), 253–275.
Raupach, M.R., 1992. Drag and drag partition on rough surfaces. Bound.-Layer Meteorol. 60 (4), 375–395.
Ravi, S., D'Odorico, P., Breshears, D.D., Field, J.P., Goudie, A.S., et al., 2011. Aeolian processes and the biosphere. Rev. Geophys. RG3001, 1–45.
Sankey, J.B., Ravi, S., Wallace, C.S.A., Webb, R.H., Huxman, T.E., 2012. Quantifying soil surface change in degraded drylands: Shrub encroachment and effects of fire and vegetation removal in a desert grassland. J. Geophys. Res.: Biogeosci. 117 (G2), 1–11.
Sankey, J.B., Law, D.J., Breshears, D.D., Munson, S.M., Webb, R.H., 2013. Employing lidar to detail vegetation canopy architecture for prediction of aeolian transport. Geophys. Res. Lett. 40 (9), 1724–1728. http://dx.doi.org/10.1002/grl.50356.

Schlichting, H., 1955. Boundary Layer Theory. Pergamon Press, New York.
Schönfeldt, H.J., von Löwis, S., 2003. Turbulence-driven saltation in the atmospheric surface layer. Meteorol. Z. 12 (5), 257–268.
Shaw, R.H., Tavangar, T., Ward, D.P., 1983. Structure of the Reynolds stress in the canopy layer. J. Climate Appl. Meteorol. 22, 1922–1931.
Smith, C.R., 1996. Coherent flow structures in smooth-wall turbulent boundary layers: facts, mechanisms and speculation. In: Ashworth, P.J., Bennett, S.J., Best, J.L., McLelland, S.J. (Eds.), Coherent Flow Structures in Open Channels. John Wiley & Sons, New York, pp. 1–39.
Sterk, G., Jacobs, A.F.G., Van Boxel, J.H., 1998. The effect of turbulent flow structures on saltation sand transport in the atmospheric boundary layer. Earth Surf. Proc. Land. 23 (10), 877–887.
Stewart, J., Parsons, A.J., Wainwright, J., Okin, G.S., Bestelmeyer, B., Fredrickson, E.L., Schlesinger, W.H., 2014. Modelling emergent patterns of dynamic desert ecosystems. Ecol. Monogr. 84 (3), 373–410.
Suter-Burri, K., Gromke, C., Leonard, K.C., Graf, F., 2013. Spatial patterns of aeolian sediment deposition in vegetation canopies: observations from wind tunnel experiments using colored sand. Aeolian Res. 8, 65–73. http://dx.doi.org/10.1016/j.aeolia.2012.11.002.
Sutton, S.L.F., McKenna-Neuman, C., 2008. Sediment entrainment to the lee of roughness elements: effects of vortical structures. J. Geophys. Res. 113, F02S09.
Thomas, D.S.G., Knight, M., Wiggs, G.F.S., 2005. Remobilization of southern African desert dune systems by twenty-first century global warming. Nature 435 (7046), 1218–1221.
Tischmacher, M., Ruck, B., 2013. Interaction of gusts and forest edges – An experimental wind-tunnel study. Forestry 86 (5), 523–532. http://dx.doi.org/10.1093/forestry/cpt029.
van Boxel, J., Sterk, G., Arens, S., 2004. Sonic anemometers in aeolian sediment transport research. Geomorphology 59 (1–4), 131–147.
von Hardenberg, J., Kletter, A.Y., Yizhaq, H., Nathan, J., Meron, E., 2010. Periodic versus scale-free patterns in dryland vegetation. Proc. Biol. Sci./Royal Soc. 277 (1688), 1771–1776.
Wainwright, J., 2009. Desert Ecogeomorphology. In: Parsons, A.J., Abrahams, A.D. (Eds.), Geomorphology of Desert Environments, second ed. Springer, Berlin, pp. 21–66.
Walker, I.J., 2005. Physical and logistical considerations of using ultrasonic anemometry in aeolian sediment transport research. Geomorphology 68, 57–76.
Walter, B., Gromke, C., Leonard, K., Clifton, A., Lehning, M., 2012. Spatially resolved skin friction velocity measurements using Irwin sensors: a calibration and accuracy analysis. J. Wind Eng. Ind. Aerodyn. 104–106, 314–321. http://dx.doi.org/10.1016/j.jweia.2012.02.018.
Wang, X., Yang, Y., Dong, Z., Zhang, C., 2009. Responses of dune activity and desertification in China to global warming in the twenty-first century. Global Planet. Change 67, 167–185.
Wasson, R.J., Nanninga, P.M., 1986. Estimating wind transport of sand on vegetated surfaces. Earth Surf. Proc. Land. 11, 505–514.
Weaver, C.M., 2008. Turbulent flow and sand dune dynamics: identifying controls on aeolian sediment transport (Unpublished Ph.D. thesis). University of Oxford.
Weaver, C.M., Wiggs, G.F.S., 2011. Field measurements of mean and turbulent airflow over a barchan sand dune. Geomorphology 128 (1–2), 32–41.
Wengle, H., Huppertz, A., Bärwolff, G., Janke, G., 2001. Manipulated transitional backward-facing step flow: an experimental and direct numerical simulation investigation. Eur. J. Mech., B/Fluids 20 (1), 25–46. http://dx.doi.org/10.1016/S0997-7546(00)01105-5.
Wiggs, G.F.S., Weaver, C.M., 2012. Turbulent flow structures and aeolian sediment transport over a barchan sand dune. Geophys. Res. Lett. 39 (5), 1–7.
Wiggs, G.F.S., Livingstone, I., Thomas, D.S.G., Bullard, J.E., 1994. Effect of vegetation removal on airflow patterns and dune dynamics in the southwest Kalahari Desert. Land Degrad. Rehabil. 5, 13–24.
Wiggs, G.F.S., Thomas, D.S.G., Bullard, J.E., Livingstone, I., 1995. Dune mobility and vegetation cover in the southwest Kalahari Desert. Earth Surf. Proc. Land. 20 (6), 515–529.
Wiggs, G.F.S., Livingstone, I., Thomas, D.S.G., Bullard, J.E., 1996. Airflow and roughness characteristics over partially-vegetated linear dunes in the southwest Kalahari Desert. Earth Surf. Proc. Land. 21, 19–34.
Wolfe, S.A., Nickling, W.G., 1993. The protective role of sparse vegetation in wind erosion. Prog. Phys. Geogr. 17, 50–68.
Wu, X., Zou, X., Zhou, N., Zhang, C., Shi, S., 2015. Deceleration efficiencies of shrub windbreaks in a wind tunnel. Aeolian Res. 16, 11–23. http://dx.doi.org/10.1016/j.aeolia.2014.10.004.
Youssef, F., Visser, S.M., Karssenberg, D., Erpul, G., Cornelis, W.M., Gabriels, D., Poortinga, A., 2012. The effect of vegetation patterns on wind-blown mass transport at the regional scale: a wind tunnel experiment. Geomorphology 159–160, 178–188. http://dx.doi.org/10.1016/j.geomorph.2012.03.023.
Yue, W., Meneveau, C., Parlange, M.B., Zhu, W., van Hout, R., Katz, J., 2007. A comparative quadrant analysis of turbulence in a plant canopy. Water Resour. Res. 43 (5), 2–15. http://dx.doi.org/10.1029/2006WR005583.